Exploring the Limits of N-Type Ultra-Shallow Junction Formation

Craig M. Polley,[†,*] Warrick R. Clarke,[†] Jill A. Miwa,[†] Giordano Scappucci,[†] Justin W. Wells,[‡] David L. Jaeger,[§] Maia R. Bischof,[§] Richard F. Reidy,[§] Brian P. Gorman,[⊥] and Michelle Simmons[†,*]

[†]School of Physics, University of New South Wales, Sydney, New South Wales 2052, Australia, [‡]Department of Physics, Norwegian University of Science and Technology (NTNU), N-7491 Trondheim, Norway, [§]Department of Materials Science and Engineering, University of North Texas, Denton, Texas 76209, United States, and [⊥]Interdisciplinary Materials Science Program, Colorado School of Mines, Golden, Colorado 80401, United States

ABSTRACT Low resistivity, near-surface doping in silicon represents a formidable challenge for both the microelectronics industry and future quantum electronic devices. Here we employ an ultra-high vacuum strategy to create highly abrupt doping profiles in silicon, which we characterize *in situ* using a four point probe scanning tunnelling microscope. Using a small molecule gaseous dopant source (PH_3) which densely packs on a reconstructed silicon surface, followed by encapsulation in epitaxial silicon, we form highly conductive dopant sheets with subnanometer control of the depth profiles. This approach allows us to test the limits of ultra-shallow junction formation, with room temperature resistivities of 780 Ω/□ at an encapsulation depth of 4.3 nm, increasing to 23 kΩ/□ at an encapsulation depth of only 0.5 nm. We show that this depth-dependent resistivity can be accounted for by a combination of dopant segregation and surface scattering.

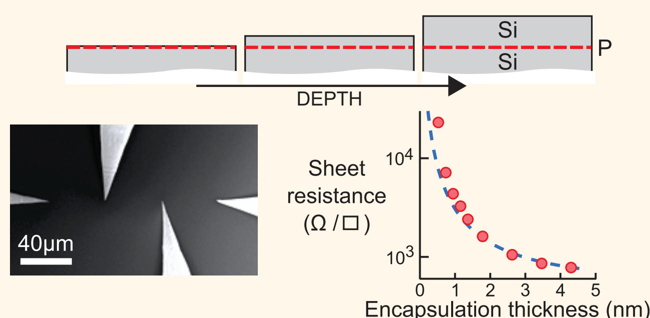

KEYWORDS: four point probe · ultra-shallow junction · delta doping

The sustained effort within the microelectronics industry to reduce device dimensions to the sub-10 nm scale poses unique technological challenges.[1,2] This includes the creation of low resistivity doping profiles for transistor source/drain extensions, which must be both shallow and abrupt to avoid short-channel effects.[3] Abrupt doping profiles are also a key element of both silicon spintronic architectures[4] and the development of an all epitaxial silicon based quantum computer.[5] The 2011 International Technology Roadmap for Semiconductors (ITRS) sets sub-8 nm depth targets by 2015,[6] which is beyond the currently demonstrated limits of mainstream ion implantation[7−14] (Figure 1). To realize the low resistivity, near-surface doping profiles required for future electronic and spintronic devices, there is active research into surface mediated, damage-free alternatives such as monolayer doping[15] (blue diamonds in Figure 1), surface transfer doping[16] and δ-doping.[17]

Controlled low-temperature epitaxy in ultra-high vacuum provides the opportunity to experimentally realize the end-point of ultra-shallow junction scaling. Using the gaseous dopant precursor phosphine (PH_3) which adsorbs in a self-limiting monolayer coverage on a clean reconstructed silicon surface, we achieve a very high surface doping density owing to the small footprint of the phosphine molecule. In contrast to both implantation and monolayer doping techniques, the subsequent annealing and silicon overgrowth steps are at low temperatures (<350 °C), resulting in negligible diffusion of dopants into the substrate. The result is a high density ($\approx 2 \times 10^{14}$ cm^{-2}), highly abrupt 2D doping profile at well controlled depths from the silicon-vacuum interface. As can be seen in Figure 1 (red stars), this allows the creation of shallow doping layers with depth and resistivity values surpassing any previously reported technique. Furthermore, this doping technique has been shown to be readily compatible with

* Address correspondence to
craig.polley@maxlab.lu.se
michelle.simmons@unsw.edu.au.

Received for review April 3, 2013
and accepted May 23, 2013.

Published online May 30, 2013
10.1021/nn4016407

© 2013 American Chemical Society

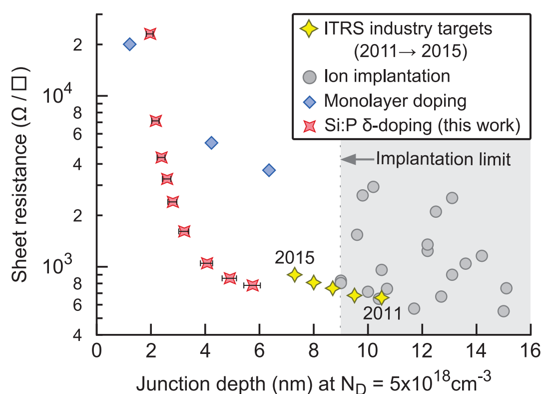

Figure 1. Depth dependent sheet resistance of a Si:P δ-doping layer. Here depth refers to the distance from the surface at which the doping density falls below 5×10^{18} cm^{-3}. For comparison, we include the 2011 ITRS targets[6] and compiled results from the literature for ultrashallow silicon doping using ion implantation[7−14] and monolayer doping.[15] Error bars in depth arise from a combination of the encapsulation rate calibration and the extrapolation of junction depth in Figure 2.

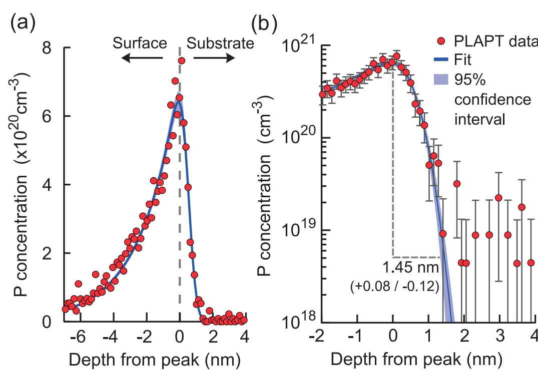

Figure 2. Depth profiling of the physical dopant distribution with PLAPT indicates both segregation into the encapsulation layer and diffusion into the substrate (a), with only the latter being important for defining the junction depth. Closer inspection of the trailing edge (b) indicates that the doping concentration falls below 5×10^{18} cm^{-3} over a distance of $\approx$1.45 nm. Details of the PLAPT measurements and the curve-fitting can be found in the Supporting Information.

lateral patterning of atomic-[5] and micrometer-scale[18] features.

As the depth of the doping layer approaches zero, it is expected that interactions with the silicon surface will become important, such as incomplete ionization,[19] surface charge transfer[20] and interface roughness scattering.[21] A full understanding of the shallow depth limit requires control of the surface condition, such that a combined ultra-high vacuum (UHV) fabrication and characterization technique is required. In a previous paper, we demonstrated how this can be accomplished using an *in situ* microscopic four-point probe (4PP) system.[22] Here we extend this work to present a detailed UHV study of the depth-dependence of Si:P δ-doping layers, allowing exploration of the limits of ultra-shallow doping in silicon. As Figure 1 demonstrates, the combination of UHV δ-doping and microscopic 4PP measurements provide access to the extreme limits of ultra-shallow doping in silicon.

For these experiments, we have used p-type Si(100) substrates, with doping densities from 0.015 to 75 Ω·cm. Silicon samples were prepared by heating to 1200 °C in UHV to remove the native oxide and obtain a Si(100) 2 × 1 surface reconstruction. The surfaces were then saturation dosed with 1.4 L of phosphine gas at room temperature and annealed to 350 °C for 60 s to substitutionally incorporate phosphorus atoms into the top layer of the silicon lattice.[23] The incorporated surface was then held at 250 °C and overgrown with epitaxial silicon from a high-resistivity (>1 kΩ·cm) sublimation cell at a growth rate of ≈0.3 nm/min. These growth parameters have been shown previously to optimize the electrical properties[24] and minimize the spreading of the doping profile.[25] At such low temperatures and having avoided the crystal lattice damage typical of implantation, dopant diffusion into the substrate is essentially negligible. With 25 nm of encapsulation, this process is known to result in full dopant activation with 2D carrier densities of $\approx 2 \times 10^{14}$ cm^{-2}.[26] The sample preparation and *in situ* four-probe measurements were performed with a commercially available Omicron Nanoprobe system. Details of the measurement technique are discussed in a previous article.[22] With four independent scanning tunneling microscope probes, we are able to measure four terminal resistances as a function of the equidistant probe separation, which is a well-known means of determining whether conduction is through the substrate or the surface doping layer.[22,27−29]

RESULTS AND DISCUSSION

Physical Profile. For a meaningful comparison with existing ultra-shallow doping literature, it is important to clearly define how the junction depth is determined. The standard definition is the distance from the surface at which the doping concentration drops below that of the bulk doped substrate, 5×10^{18} cm^{-3} for conventional 10 mΩ·cm substrates. In our samples, we are burying a dopant sheet, so that the junction depth consists of the encapsulation thickness plus the additional distance required for the trailing edge of the phosphorus profile to fall below 5×10^{18} cm^{-3}. While the initial placement of dopants is by surface adsorption and is hence a zero depth layer, the subsequent processes of dopant incorporation and encapsulation will result in some amount of diffusion into the substrate and segregation into the encapsulation layer. The low temperatures used for dopant incorporation (350 °C) and silicon encapsulation (250 °C) are expected to result in negligible diffusion, and this is verified by careful depth profiling measurements.

In Figure 2, we show a phosphorus depth profile measurement of a typical Si:P δ-doped layer. Due to the

known broadening artifacts arising from sputter-based profiling techniques,[30,31] we have obtained sputter-free pulsed laser atom probe tomography (PLAPT) in addition to secondary ion mass spectrometry (SIMS). A direct comparison of measurements with both techniques is provided in the Supporting Information. PLAPT employs laser pulses with a locally large surface electric field to sequentially field evaporate ions from the sample surface, and is well suited to studies of nanoscale doping layers.[32] As shown in Figure 2a, both segregation and diffusion are apparent, and the doping profile is well described by an exponentially modified Gaussian fit. The segregation behavior agrees with previous studies, and will be discussed later. To evaluate the diffusion edge, in Figure 2b we replot part of the profile on a logarithmic scale. We also include sampling error bars corresponding to a binomial confidence interval of 1.96σ (95%). The sampling error rapidly increases for concentrations below $\approx 5 \times 10^{19}$ cm^{-3} where data points correspond to only a few detected P atoms. This necessitates examining the Gaussian tail of the fit to determine the depth at which the phosphorus concentration reaches 5×10^{18} cm^{-3}. Measurements of similar samples with SIMS confirm that there are no `kinks' in the phosphorus profile and hence this extrapolation is valid (see Supporting Information). As indicated in Figure 2b, the phosphorus concentration reaches 5×10^{18} cm^{-3} at a distance of only $\approx$1.45 nm from the profile peak.

We note that for such a sharp doping profile it is not clear whether Figure 2 represents the true doping profile or a resolution limit of the PLAPT technique. Several processes may contribute to such a resolution limit, including local variations in evaporation fields between silicon and phosphorus atomic species, field- and thermally induced surface diffusion, field penetration beyond the tip surface and correlated ion evaporation.[33] We note however that here we obtain a trailing edge decay length of $\approx$0.8 nm/decade, in agreement with previous measurements of boron δ-doped silicon[33] and isotopically enriched heterostructures of silicon.[34] For the present purposes, we simply assume that the $\approx$1.45 nm depth obtained from Figure 2b represents an upper bound. On this basis, we may then define the junction depth of our samples to be the thickness of the grown encapsulation layer plus an additional $\approx$1.45 nm diffusion tail.

Electrical Profile. Ultimately, for device applications it is not the distribution of dopants but of free carriers which is important. Classically this is determined by a drift-diffusion equilibrium, captured by the Debye length screening parameter. The scaling down of substrate resistivities in microelectronics manufacturing is motivated by reducing the Debye length ($L_D \propto 1/n_d$) and hence the electrical width of doping profiles. However, for the narrow, heavily doped layers described here, there is justification for considering the carrier distribution to be a quantum confined 2D layer, in which case the substrate doping level has far less bearing on the electrical depth. Weak localization is routinely observed in low temperature magnetotransport measurements of these Si:P δ-layers,[24] which is a signature of diffusive 2D conduction. At room temperature a two-dimensional electron state can be observed by angle-resolved photoemission,[35] in agreement with atomistic tight-binding calculations which predict a room temperature degenerate electron state with a Fermi level $\approx$100 meV below the bulk conduction band.[36]

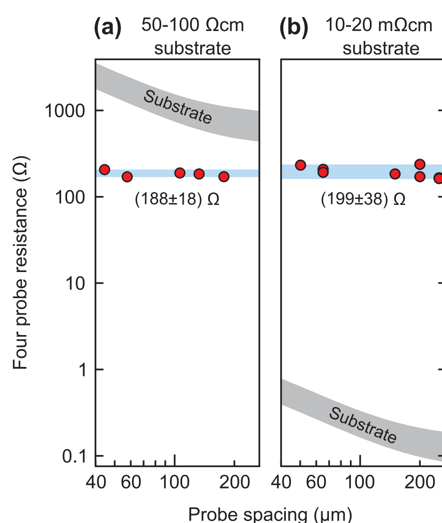

Figure 3. Spacing dependent 4PP measurements of Si:P δ-layers formed on (a) high resistivity 50–100 $\Omega\cdot$cm and (b) low resistivity 10–20 m$\Omega\cdot$cm substrates yield identical results. Gray curves indicate the expected 4PP resistance of each substrate, while the blue bands indicate the range of the measured 2D resistances.

Regardless of what governs the free carrier distribution in these samples, it is important to establish whether our resistivity measurements are influenced by the substrate doping level. All electrical measurements presented here are taken on 7 $\Omega\cdot$cm p-type substrates, with the exception of Figure 3 where we show measurements of a 5 nm deep doping layer formed on p-type substrates of radically different doping levels (nominally 50–100 $\Omega\cdot$cm and 10–20 m$\Omega\cdot$cm). Despite changing the substrate resistivity by 3 orders of magnitude, we observe no significant difference in the four-terminal resistance measurements. The measured resistances are independent of probe separation (a signature of 2D conduction) and commensurate with those expected from shallow Si:P δ-layers.[22] Previously, we demonstrated similar results when using n-type substrates, but noted that for a 20 m$\Omega\cdot$cm substrate, the δ-layer was not measurable due to excessive current leakage through the substrate.[22] In Figure 3 this is not the case, which can be attributed to the presence of a depletion layer from the p–n junction blocking current flow into the substrate.

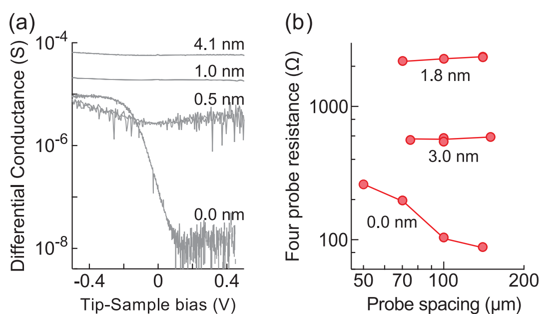

Figure 4. Depth-dependent electrical characterization of Si:P δ-doped silicon. The current–voltage characteristics of an individual probe-to-sample contact (a) show an abrupt elimination of rectification at an encapsulation depth of only 0.5 nm. Spacing dependent four-probe resistance measurements (b) demonstrate that this transition is from conduction through the substrate ($R \propto 1/d$) to conduction through the dopant sheet (R = constant), with a decreasing sheet resistivity for increasing encapsulation thicknesses. The uncertainty in thickness values arising from growth rate calibration is ≈5%.

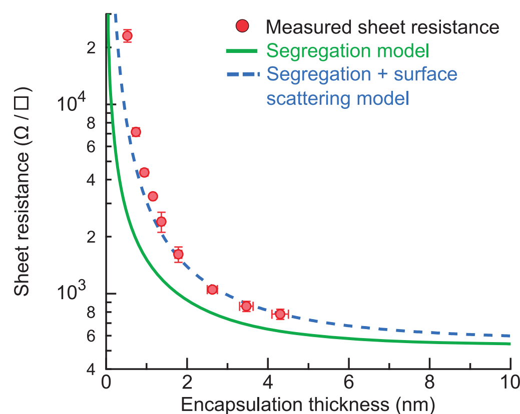

Figure 5. A model of the depth-dependent δ-layer conductivity based on dopant segregation. By accounting for a finite segregation length, we infer a depth-dependent conductivity (green solid trace) which is qualitatively similar to the experimental measurements. Including a $1/d$ surface scattering term in the segregation model (blue dashed trace) greatly improves the match to experimental data.

Figure 3 confirms that despite the use of lightly doped (7 Ω·cm) substrates, our depth dependence measurements are relevant for the heavier doped substrates used in commercial manufacturing.

Depth Dependence. Depth dependent electrical measurements were performed by first phosphine dosing the silicon surface (1.4 L) and thermally incorporating the dopants (350 °C), then performing repeated cycles of 250 °C silicon overgrowth and room temperature 4PP measurements. In this way within any given data set, we follow the evolution of a single sample as the dopant plane is buried progressively deeper. The silicon growth rate is very slow (≈0.3 nm/min) and stable, such that 0.5 nm growth steps are readily achievable. Following the completion of the *in situ* measurements, samples are overgrown with an additional >50 nm of silicon to allow confirmation of the growth rate by both atomic force microscopy and SIMS.

In Figure 4, we present the results of two different depth-dependent experiments, which are representative of repeatable behavior seen in all samples. Figure 4a shows the tip-to-sample current–voltage behavior (numerically differentiated to conductance), while Figure 4b shows spacing dependent four-probe resistance measurements. In both cases, we see that the dopant layer is not electrically active for encapsulation thicknesses of less than 0.5 nm, with the measurements instead resembling those of a clean silicon substrate. Specifically, the tip–sample contacts are highly rectifying while the 4PP measurements show a resistance inversely proportional to the probe spacing. Once the encapsulation thickness exceeds 0.5 nm there is a dramatic change, with the tip-to-sample rectification being eliminated and the four-terminal resistance becoming independent of probe spacing. These observations are consistent with the dopant layer becoming electrically active and dominating conduction. With increasing encapsulation the dopant layer becomes progressively more conductive, which is also clearly seen in Figure 1. The conductivity at sub 5 nm depths is remarkable, which bodes well for technological applications.

Further analysis allows us to comment on the potential mechanisms driving the increase in sheet resistance shown in Figure 1. In Figure 5, we demonstrate that most of the observed behavior can be qualitatively explained by a combination of the finite segregation length of the dopants and a simple surface scattering model. In Figure 2, it was seen that there is some degree of dopant segregation as the encapsulation layer is grown. Using a simple incorporation probability model, the segregation behavior can be captured with the single parameter Δ, which describes the $1/e$ decay length of the dopants toward the growth front.[37] It follows that for encapsulation depths comparable to Δ, a non-negligible fraction of the dopants will reside on the surface, and according to the measurements in Figure 4 will be electrically inactive. This leads to a description of the resistivity, ρ, as a function of encapsulation depth, d:

$$\rho(d) = \rho_{\infty}(1 - e^{(-d/\Delta)}) \tag{1}$$

where ρ_{∞} is the limiting value of sheet resistance found for deep (d > 10 nm) encapsulations of 540 Ω/□. The segregation length Δ is determined from the PLAPT data in Figure 2 to be (2.41 ± 0.05) nm, in agreement with previously reported SIMS measurements[25] as well as more recent SIMS data provided in the Supporting Information. Using these values with eq 1 produces the solid green trace in Figure 5.

While this segregation model captures much of the depth dependence trend, it can be improved by including surface scattering using a simple

Fuchs model:[21]

$$\rho(d) = \rho_\infty\left(1+\frac{3}{8}\frac{\lambda(1-p)}{d}\right) \quad (2)$$

where p is the specularity parameter, λ is the electron mean free path and d is the thickness of the conducting region. Here ρ_∞ refers to the sheet resistance in the absence of any surface scattering. On the basis of previous studies, a mean free path of $\approx$10 nm is expected,[38,39] while primarily specular scattering ($p \rightarrow 1$) is expected based on the low surface roughness of the epitaxial encapsulation layer.

In Figure 5, we plot this modified sheet resistance calculation combining both segregation and surface scattering (blue dashed trace), and find a greatly improved description of the experimental data for a mean free path of 10 nm and specularity parameter of 0.73. These values are plausible, suggesting that the use of Fuchs' model is appropriate here. However, we note that several other physical effects could also be expected in this system, and should be included in a more comprehensive model before drawing quantitative conclusions. These include surface charge trapping,[20,40] image charge interactions due to the silicon-vacuum dielectric mismatch,[41] and modifications to the donor confinement potential.[19] These additional interactions are nontrivial to treat, and beyond the scope of the present investigation.

CONCLUSIONS

In summary, we have shown that the PH_3 surface doping technique offers a means of creating ultrashallow doping layers in silicon with low resistivity, high abruptness and subnanometer depth control. Such thin, high density layers result in quantum confinement of the free carriers, such that despite the use of relatively conductive (7 $\Omega\cdot$cm) substrates the doping layers are as narrow electrically as they are physically. We directly demonstrate that the layer resistivity does not change when the substrate doping is varied over several orders of magnitude. In contrast, the resistivity increases sharply as encapsulation depths are reduced below 5 nm, eventually becoming electrically inactive at depths below 0.5 nm. This behavior has been explained in terms of dopant segregation during encapsulation, with additional corrections which can be captured by a simple surface roughness scattering model. Our findings demonstrate that the combination of UHV monolayer doping and *in situ* 4PP characterization provide the means of exploring ultrashallow junction scaling limits, a topic of interest for both fundamental research and the advancement of microelectronic manufacturing.

METHODS

Sample Preparation. A commercially available UHV STM (Omicron Nanoprobe) was used to fabricate and characterize the samples. The sample preparation is discussed in detail in the main manuscript. Heating was performed by passing a direct-current through the sample, with the temperature monitored by an *ex situ* optical pyrometer.

Electrical Characterization. One- and two-terminal measurements are carried out using a Keithley 236-SMU; four-terminal measurements employed a Keithley 6514 electrometer in addition. An *in situ* scanning electron microscope was used to verify the probe positioning. A detailed discussion of the four-probe measurement process can be found in an earlier paper.[22]

Depth Profiling. Pulsed laser atom probe tomography was performed at the University of North Texas Center for Advanced Research and Technology (CART) using a Local Electrode Atom Probe (LEAP) 3000X HR (CAMECA Atom Probe Technology Center, Madison, WI) laser pulsed local electrode atom probe with a reflectron lens. Samples were analyzed at a base temperature of 50 K in laser pulsed field evaporation mode using a pulsed laser with a wavelength of 532 nm, pulse width of 10 ps, pulse frequency of 160 kHz, laser energy of (0.2−0.3) nJ and an evaporation rate of (0.001−0.005) ions/pulse.

After removal from UHV and transport to the CART laboratory, the Si:P δ-doped thin film samples were coated with a protective 40 nm amorphous Cr film sputter deposited using a broad ion beam (10 kV, 450 μA) (Gatan 682 PECS, Pleasanton, CA). The coated samples were stored under Ar before transfer to a focused ion beam/scanning electron microscope (FIB/SEM) dual-beam system (FEI Nova 200 Nanolab, Hillsboro, OR) to prepare PLAPT-compatible samples using established methods. After transfer into the FIB/SEM, a bar of Pt was deposited using the ion beam over a site specific region of interest of the sample surface. A wedge containing the region of interest and Pt bar was milled free from the chip using the FIB. An *in situ* micromanipulator (Omniprobe Autoprobe 200, Dallas, TX) was attached to the wedge using FIB deposited Pt and then cut free. Individual 3 μm wide segments were mounted to Si microtip posts (CAMECA Atom Probe Technology Center, Madison, WI). A sequence of annular milling patterns with progressively smaller inner diameters were used to shape and then roughly sharpen individual tips. A final series of 5 kV focused ion beam scans were applied to remove surface damage incurred during the FIB milling process and shape the end of the apex to an approximate hemispherical shape. The final PLAPT profiles were sampled perpendicular to the doping layer from 30 $\times$ 30 nm^2 areas in 0.13 nm thick slices. This small sampling region (necessary to create sufficiently strong electric fields for ion evaporation) is responsible for the greatly reduced resolution at phosphorus concentrations below 1 $\times$ 10^{19} cm^{-3}.

The resulting tomographic atom probe data was reconstructed and analyzed using the Integrated Visualization and Analysis Software (IVAS 3.6.4) program (CAMECA Atom Probe Technology Center, Madison, WI). Standard reconstruction parameters for LEAP 3000X HR instruments and silicon were used assuming a hemispherical tip shape and a voltage dependent tip radius evolution. The field enhancement factor (kF) was the only parameter varied during the reconstruction process. It was adjusted to produce relatively flat P enriched layers, Si interplanar spacings measured using spatial distribution maps (SDM) that agree with those for Si (100) surfaces, and P densities and layer locations that agree with transmission electron microscopy (TEM) and secondary ion mass spectroscopy (SIMS) structural and chemical measurements.

Conflict of Interest: The authors declare no competing financial interest.

Acknowledgment. W.R.C. acknowledges funding from the Australian Research Council in the form of an Australian Post-Doctoral Fellowship. M.S. acknowledges an Australian

Government Federation Fellowship. D.L.J., M.R.B., R.F.R., and B.P. G. acknowledge support from the Defense Advanced Research Project Agency, Space and Naval Warfare Center, San Diego, and the Emerging Technology Fund of the State of Texas under contract N66001-08-C-2040. The authors are grateful to John N. Randall of Zyvex Laboratories for helpful discussions.

Supporting Information Available: Details of the PLAPT fitting procedure, together with a comparison of SIMS and PLAPT measurements. This material is available free of charge *via* the Internet at http://pubs.acs.org.

REFERENCES AND NOTES

1. Peercy, P. S. The Drive to Miniaturization. *Nature* **2000**, *406*, 1023–1026.
2. Vogel, E. Technology and Metrology of New Electronic Materials and Devices. *Nat. Nanotechnol.* **2007**, *2*, 25–32.
3. Ieong, M.; Doris, B.; Kedzierski, J.; Rim, K.; Yang, M. Silicon Device Scaling to the Sub-10-nm Regime. *Science* **2004**, *306*, 2057–2060.
4. Jansen, R. Silicon Spintronics. *Nat. Mater.* **2012**, *11*, 400–408.
5. Fueschle, M.; Miwa, J. A.; Mahapatra, S.; Ryu, H.; Lee, S.; Warschkow, O.; Hollenberg, L. C. L.; Klimeck, G.; Simmons, M. Y. A Single-Atom Transistor. *Nat. Nanotechnol.* **2012**, *7*, 242–246.
6. Semiconductor Industry Association, *International Technology Roadmap for Semiconductors* **2011**, Table FEP12; available at http://www.itrs.net
7. Zschätzsch, G.; Vanderworst, W.; Hoffmann, T.; Goossens, J.; Everaert, J.-L.; del Agua Borniquel, J. I.; Poon, T. Basic Aspects of the Formation and Activation of Boron Junctions Using Plasma Immersion Ion Implantation. *Int. Conf. Ion Implant. Technol., 2008* **2008**, *1066*, 461–464.
8. Shao, Y.; Hautala, J.; Larson, L.; Jain, A. Dopant Activation and Defect Analysis of Ultra-Shallow Junctions Made by Gas Cluster Ion Beams. *Int. Conf. Ion Implant. Technol., 2008* **2008**, *1066*, 411–414.
9. Jin, C. G.; Sasaki, Y.; Okashita, K.; Tamura, H.; Ito, H.; Mizuno, B. Ultra Shallow p^+/n Junction Formation by Plasma Doping (PD) and Long Pulse All Solid-State Laser Annealing (ASLA) with Selective Absorption Modulation. *Nucl. Instrum. Methods Phys. Res., Sect. B* **2005**, *237*, 58–61.
10. Hatem, C.; Renau, L.; Godet, L.; Kontos, A.; Papasouliotis, G.; England, J.; Arevalo, E. Approaches to USJ Formation beyond Molecular Implantation. *AIP Conf. Proc.* **2008**, *1066*, 399–402.
11. Heo, S.; Hwang, H.; Cho, H. T; Krull, W. A. Ultrashallow (<10nm) p^+/n Junction Formed by $B_{18}H_{22}$ Cluster Ion Implantation and Excimer Laser Annealing. *Appl. Phys. Lett.* **2006**, *89*, 243516.
12. Kalra, P.; Majhi, P.; Tseng, H.-H.; Jammy, R.; King Liu, T.-J. Infusion Doping for Sub-45 nm CMOS Technology Nodes. *AIP Conf. Proc.* **2008**, *1066*, 407–410.
13. Papasouliotis, G. D.; Godet, L.; Singh, V.; Miura, R.; Ito, H. Formation of Ultra-Shallow Junctions by Advanced Plasma Doping Technique. *AIP Conf. Proc.* **2011**, *1321*, 146–149.
14. Hara, S.; Tanaka, Y.; Fukaya, T.; Matsumoto, S.; Suzuki, T.; Fuse, G.; Kudo, T.; Sakuragi, S. Ultra-Shallow P^+/N Junction Formation in Si Using Low Temperature Solid Phase Epitaxy Assisted with Laser Activation. *AIP Conf. Proc.* **2008**, *1066*, 79–82.
15. Ho, J. C; Yerushalmi, R.; Smith, G.; Majhi, P.; Bennett, J.; Halim, J.; Faifer, V. N; Javey, A. Wafer-Scale, Sub-5 nm Junction Formation by Monolayer Doping and Conventional Spike Annealing. *Nano Lett.* **2009**, *9*, 725–730.
16. Chen, W.; Qi, D.; Gao, X.; Wee, A. T. S. Surface Transfer Doping of Semiconductors. *Prog. Surf. Sci.* **2009**, *84*, 279–321.
17. Scappucci, G.; Capellini, G.; Klesse, W. M; Simmons, M. Y. Preparation of the Ge(001) Surface towards Fabrication of Atomic-Scale Germanium Devices. *Nanotechnology* **2011**, *22*, 145604.
18. Hallam, T.; Butcher, M. J; Goh, K. E. J; Reuß, F. J; Simmons, M. Y. Use of a Scanning Electron Microscope to Pattern Large Areas of a Hydrogen Resist for Electrical Contacts. *J. Appl. Phys.* **2007**, *102*, 034308.
19. Mol, J. A.; Salfi, J.; Miwa, J. A.; Simmons, M. Y.; Rogge, S. Interplay between Quantum Confinement and Dielectric Mismatch for Ultra-Shallow Dopants. *arXiv* 1303.2712. arXiv.org e-Print archive. http://arxiv.org/abs/1303.2712.
20. Song, F.; Wells, J. W; Handrup, K.; Li, Z. S; Bao, S. N; Schulte, K.; Ahola-Tuomi, M.; Mayor, L. C; Swarbrick, J. C; Perkins, E. W; *et al.* Direct Measurement of Electrical Conductance Through a Self-Assembled Molecular Layer. *Nat. Nanotechnol.* **2009**, *4*, 373–376.
21. Sambles, J. R. The Resistivity of Thin Metal Films. *Thin Solid Films* **1983**, *106*, 321–331.
22. Polley, C. M; Clarke, W. R; Miwa, J. A; Wells, J. W.; Simmons, M. Y. Microscopic Four-Point-Probe Resistivity Measurements of Shallow, High Density Doping Layers in Silicon. *Appl. Phys. Lett.* **2012**, *101*, 262105.
23. Schofield, S. R; Curson, N. J.; Simmons, M. Y; Reuß, F. J; Hallam, T.; Oberbeck, L.; Clark, R. G. Atomically Precise Placement of Single Dopants in Si. *Phys. Rev. Lett.* **2003**, *91*, 136104.
24. Goh, K. E. J; Oberbeck, L.; Simmons, M. Y; Hamilton, A. R; Clark, R. G. Effect of Encapsulation Temperature on Si:P δ-Doped Layers. *Appl. Phys. Lett.* **2004**, *85*, 4953.
25. Oberbeck, L.; Curson, N. J; Hallam, T.; Simmons, M. Y; Bilger, G.; Clark, R. G. Measurement of Phosphorus Segregation in Silicon at the Atomic Scale Using Scanning Tunneling Microscopy. *Appl. Phys. Lett.* **2004**, *85*, 1359.
26. McKibbin, S. R; Clarke, W. R; Fuhrer, A.; Reusch, T. C. G; Simmons, M. Y. Investigating the Regrowth Surface of Si:P δ-Layers Toward Vertically Stacked Three Dimensional Devices. *Appl. Phys. Lett.* **2009**, *95*, 233111.
27. Perkins, E.; Barreto, L.; Wells, J.; Hofmann, P. Surface-Sensitive Conductivity Measurement using a Micro Multi-point Probe Approach. *Rev. Sci. Instrum.* **2013**, *84*, 033901.
28. Hofmann, Ph.; Wells, J. W. Surface-Sensitive Conductance Measurements. *J. Phys.: Condens. Matter* **2009**, *21*, 013003.
29. Matsuda, I.; Liu, C.; Hirahara, T.; Ueno, M.; Tanikawa, T.; Kanagawa, T.; Hobara, R.; Yamazaki, S.; Hasegawa, S. Electron-Phonon Interaction and Localization of Surface-State Carriers in a Metallic Monolayer. *Phys. Rev. Lett.* **2007**, *99*, 146805.
30. Baboux, N.; Dupuy, J. C.; Prudon, G.; Holliger, P.; Laugier, F.; Papon, A. M.; Hartmann, J. M. Ultra-Low Energy SIMS Analysis of Boron Deltas in Silicon. *J. Cryst. Growth* **2002**, *245*, 1–8.
31. Kelly, T. F.; Miller, M. K. Atom Probe Tomography. *Rev. Sci. Instrum.* **2007**, *78*, 031101.
32. Scappucci, G.; Klesse, W. M; Hamilton, A. R; Capellini, G.; Jaeger, D. L; Bischof, M. R; Reidy, R. F; Gorman, B. P; Simmons, M. Y. Stacking of 2D Electron Gases in Ge Probed at the Atomic Level and its Correlation to Low-Temperature Magnetotransport. *Nano Lett.* **2012**, *12*, 4953–4959.
33. Cadel, E.; Vurpillot, F.; Lardé, R.; Duguay, S.; Deconihout, B. Depth Resolution Function of the Laser Assisted Tomographic Atom Probe in the Investigation of Semiconductors. *J. Appl. Phys.* **2009**, *106*, 044908.
34. Shimizu, Y.; Kawamura, Y.; Uematsu, M.; Tomita, M.; Kinno, T.; Okada, N.; Kato, M.; Uchida, H.; Takahashi, M.; Ito, H.; *et al.* Depth and Lateral Resolution of Laser-Assisted Atom Probe Microscopy of Silicon Revealed by Isotopic Heterostructures. *J. Appl. Phys.* **2011**, *109*, 036102.
35. Miwa, J. A; Hofmann, P.; Simmons, M. Y; Wells, J. W. Direct Measurement of the Band Structure of a Buried Two-Dimensional Electron Gas. *Phys. Rev. Lett.* **2013**, *110*, 136801.
36. Ryu, H.; Lee, S.; Klimeck, G. A Study of Temperature-Dependent Properties of N-Type δ-Doped Si Band-Structures in Equilibrium. *IEEE Proceedings of the 13th International Workshop on Computational Electronics*; Birck and NCN Publications: West Lafayette, IN, 2009; pp 1−4.
37. Nützel, J. F; Abstreiter, J. F. Segregation and Diffusion on Semiconductor Surfaces. *Phys. Rev. B* **1996**, *53*, 13551–13558.

38. Reusch, T. C. G.; Goh, K. E. J.; Pok, W.; Lo, W.-C. N.; McKibbin, S. R.; Simmons, M. Y. Morphology and Electrical Conduction of Si:P δ-Doped Layers on Vicinal Si(001). *J. Appl. Phys.* **2008**, *104*, 066104.
39. Goh, K. E. J.; Oberbeck, L.; Simmons, M. Y.; Hamilton, A. R.; Butcher, M. J. Influence of Doping Density on Electronic Transport in Degenerate Si:P δ-Doped Layers. *Phys. Rev. B* **2006**, *73*, 035401.
40. Clarke, W. R.; Zhou, X. J.; Fuhrer, A.; Reusch, T. C. G.; Simmons, M. Y. The Effect of Surface Proximity on Electron Transport Through Ultra-Shallow δ-Doped Layers in Silicon. *Physica E* **2008**, *40*, 1566–1568.
41. MacMillen, D. B.; Landman, U. Variational Solutions of Simple Quantum Systems Subject to Variable Boundary Conditions. II. Shallow Donor Impurities Near Semiconductor Interfaces: Si, Ge. *Phys. Rev. B* **1984**, *29*, 4524–4533.